ISSN 0023-1584, Kinetics and Catalysis, 2009, Vol. 50, No. 1, pp. 48–56. © Pleiades Publishing, Ltd., 2009.
Original Russian Text © T.Yu. Kardash, L.M. Plyasova, V.M. Bondareva, T.V. Andrushkevich, A.V. Ishchenko, Yu.A. Chesalov, L.S. Dovlitova, 2009, published in Kinetika i Kataliz, 2009, Vol. 50, No. 1, pp. 54–62.

FIFTY YEARS
OF THE BORESKOV INSTITUTE OF CATALYSIS

Effect of Thermal Treatment Conditions on the Phase Composition and Structural Characteristics of V–Mo–Nb–O Catalysts

T. Yu. Kardash, L. M. Plyasova, V. M. Bondareva, T. V. Andrushkevich, A. V. Ishchenko, Yu. A. Chesalov, and L. S. Dovlitova

Boreskov Institute of Catalysis, Siberian Branch, Russian Academy of Sciences, Novosibirsk, 630090 Russia
e-mail: pls@catalysis.nsk.su

Received February 27, 2008

Abstract—The formation of an active phase in V–Mo–Nb oxide catalysts for the selective oxidation and ammoxidation of ethane during thermal treatment in air and in helium was studied using high-temperature in situ and ex situ X-ray diffraction analysis, transmission electron microscopy, IR spectroscopy, and the differential dissolution method. It was found that, in thermal treatment below 500°C, the formation occurred through the same irreversible steps with the formation of a unidimensionally ordered layered compound with structure elements like Mo_5O_{14} regardless of the calcination atmosphere. Above 500°C, the formation of crystalline phases took place; the composition and structure of these phases depended on the atmosphere of thermal treatment. The unidimensionally ordered V–Nb–Mo oxide with structure elements like Mo_5O_{14} exhibited the best catalytic properties.

DOI: 10.1134/S0023158409010078

INTRODUCTION

New raw material sources for the production of oxygen- and nitrogen-containing derivatives of ethylene and propylene should be found because, on the one hand, the cost of these hydrocarbons is increasing and, on the other hand, they are increasingly being used in the manufacture of polymers. Light (C_2–C_3) paraffins are the most attractive alternative raw materials because they are accessible and inexpensive [1–4].

After the pioneering work by Thorsteinson et al. [5], who demonstrated the high activity of catalysts based on mixed molybdenum and vanadium oxides with the additives of transition metal oxides in the selective oxidation of ethane, studies of the multicomponent Mo–V–X–O (X = Nb [6–13], Te, Sb, W, Bi, Al, and Ga [14–19]) and Mo–V–Nb–X–O (X = Te and Sb) [20–25] systems have intensified.

This work was devoted to V–Mo–Nb oxide catalysts, which are active in the low-temperature oxidation of ethane to ethylene [5–8, 10–13], acetonitrile [9], and acetic acid [5, 8, 10, 13, 26–28].

The set of phases forming in these catalysts depends on the composition and preparation conditions, in particular, thermal treatment conditions. The V–Mo–Nb oxide catalysts were calcined at relatively low temperatures (350–425°C). In this case, poorly crystallized compounds were formed [5, 8, 13]; because of this, the phase composition was difficult to determine. In the ternary V–Mo–Nb oxide system, solid solutions of vanadium and (or) niobium based on molybdenum oxides with the structures Mo_5O_{14} and $Mo_{18}O_{52}$ were detected along with the phases of individual compounds such as $V_6Mo_4O_{25}$ [5], $V_9Mo_6O_{40}$ [5, 13], and $Mo_3Nb_2O_{11}$ [6, 13]. Published data on the genesis of the V–Mo–Nb oxide catalysts are insufficient, and data concerning optimum thermal treatment conditions (temperature and atmosphere) are contradictory. For example, thermal treatment was performed at 400°C in a flow of air [5–7, 9, 11, 12]. Under these conditions, an active phase was formed, which was characterized by a peak at d = 4.00 Å in the X-ray diffraction pattern. Calcination in a reducing atmosphere (for example, ethylene [5] or an H_2–N_2 mixture [11]) was accompanied by the formation of MoO_2, which impaired catalytic properties [5, 15]. At the same time, it was noted [8, 10, 13] that the formation of more active catalysts occurred on calcination in an inert atmosphere of N_2. In this case, it was hypothesized that a V- and (or) Nb-containing θ-oxide of molybdenum ($Mo_{1-x}Me_xO_{2.8}$) with the Mo_5O_{14}-type structure [29], which crystallized at a temperature higher than 550°C, was active.

Earlier [9], we found that the active phase of V–Mo–Nb oxide catalysts with the formula $V_{0.3}Mo_1Nb_x$ (x = 0.05–0.27) in the ammoxidation of ethane is the compound with variable composition $V_{0.23\pm0.03}Mo_1Nb_xO_y$ (x = 0.2–0.37). This compound is formed based on the matrix of a binary Nb–Mo compound [30] with the Mo_5O_{14}-type structure (see insert in Fig. 1). In addition to the above compound, the phases of MoO_3 and V_2MoO_8 were present in the samples. As the niobium content was increased, the amount of the ternary

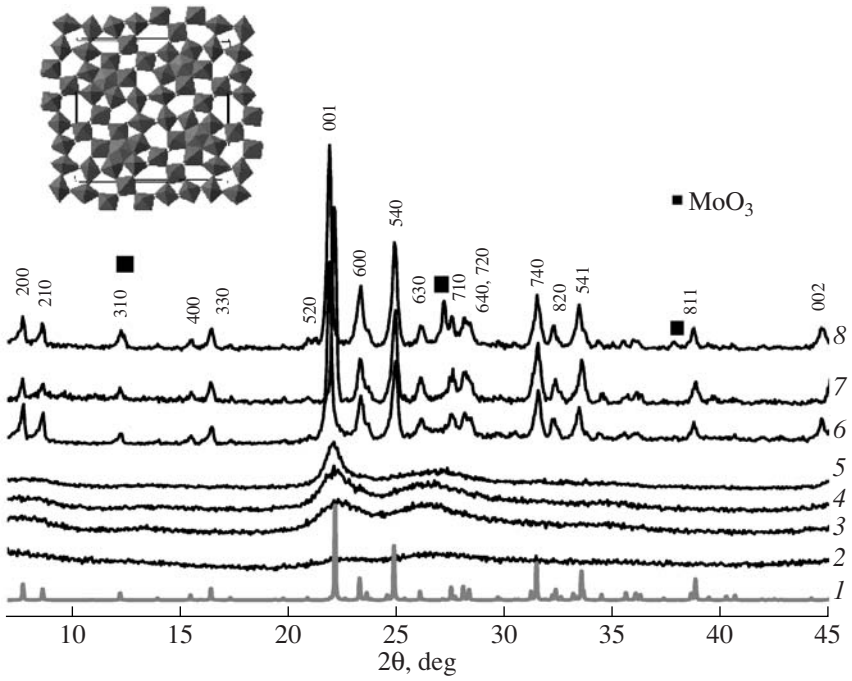

Fig. 1. (*1*) Theoretical X-ray diffraction pattern of the Mo_5O_{14}-type structure and diffraction patterns of $V_{03}MoNb_{0.37}O_x$ obtained in situ in air at temperatures of (*2*) 180, (*3*) 300, (*4*) 400, (*5*) 500, (*6*) 550, (*7*) 600, and (*8*) 650°C: (■) MoO_3; reflections from the Mo_5O_{14}-type phase are not labeled.

V–Mo–Nb compound monotonically increased and reached a maximum in the sample of $V_{0.3}Mo_1Nb_{0.27}$ [9].

The aim of this work was to study the effect of thermal treatment conditions on the formation of the active component phase and on the structural characteristics of compounds formed upon thermal treatment.

EXPERIMENTAL

In the molybdenum oxide Mo_5O_{14}, Mo^{5+}/Mo^{6+} = 0.67 [29]; in the previously studied V–Mo–Nb catalysts [9], the ratio $(V^{5+} + Nb^{5+})/Mo^{6+}$ varied from 0.35 to 0.57. To prevent the formation of impurity phases and to eliminate their effect on the formation of the active component, we prepared a model sample of $V_{0.3}Mo_1Nb_{0.37}O_x$ with the same ratio between hexavalent (Mo^{6+}) and pentavalent ($V^{5+} + Nb^{5+}$) cations as that in Mo_5O_{14}.

The sample of $V_{0.3}Mo_1Nb_{0.37}O_x$ was prepared by mixing the solutions of ammonium paramolybdate and ammonium metavanadate with niobium oxalate followed by drying in air at 180°C for 15 h; then, it was calcined in a flow of air or in helium over the temperature range of 400–650°C for 4–7 h.

The phase composition of the samples was determined on a Bruker D8 diffractometer (CuK_α radiation) using the parallel-beam geometry.

In situ experiments were performed in an HTK16 high-temperature chamber (Anton Paar, Austria) over a temperature range from 25 to 650°C in air or helium. Samples prepared in accordance with the above procedure and dried in air at 180°C were used in the in situ studies.

The chemical composition of compounds formed in the system was determined by differential dissolution [31] with the use of an inductively coupled plasma atomic emission spectrometer.

The catalytic properties of samples were determined in the ammoxidation of ethane using a flow-circulation setup with the chromatographic analysis of the reaction mixture components. The tests were performed at 400°C in a reaction mixture containing 5 vol % C_2H_6, 6 vol % NH_3, and 83 vol % N_2 with a catalyst fraction of 0.25–1 mm.

Electron micrographs were obtained on a JEM-2010 electron microscope (JEOL, Japan) with a lattice resolution of 1.4 Å at a maximum voltage of 200 kV. The microscope was also equipped with an attachment for local energy-dispersive chemical analysis (EDAX spectrometer).

IR spectra were measured on a BOMEM-MB-102 spectrometer; a sample portion (2 mg) was pelletized with KBr.

RESULTS

Tables 1–3 and Figs. 1–4 summarize the experimental results.

Table 1. Differential dissolution and X-ray diffraction data for $V_{0.3}MoNb_{0.37}O_x$ depending on thermal treatment conditions

Thermal treatment conditions		X-ray diffraction data	Differential dissolution data		
T, °C	atmosphere		amount of the V–Mo–Nb–O_x phase, %	cationic composition of the V–Mo–Nb–O_x phase, Mo/Nb/V	cationic compositions and amounts of other phases
300	air	Unidimensionally ordered phase with d = 4.00 Å	56.7	1/0.54/0.19	34.7% $Mo_1V_{0.24–0.58}O_x$ 8.6% Σ*
400	″	Unidimensionally ordered phase with d = 4.00 Å	73.6	1/0.49/0.22	20.7% $Mo_1V_{0.34}O_x$ 5.7% Σ
550	″	Structure of the Mo_5O_{14} type	95.2	1/0.36/0.27	4.8% Σ
650	″	Structure of the Mo_5O_{14} type and MoO_3 (traces)	95.3	1/0.34/0.27	4.7% Σ
650	He + 0.3%O_2	Structure of the Mo_5O_{14} type, MoO_3 (traces), and $Nb_{18}V_4O_{55}$ (traces)	96.2	1/0.37/0.28	3.8% Σ
550	He	Unidimensionally ordered phase with d = 4.00 Å and $(V_xMo_{1-x})O_2$	87.7	1/0.41/0.20	8.7% $Mo_1V_1O_x$ 3.6% Σ
650	″	Unidimensionally ordered phase with d = 4.00 Å, $(V_xMo_{1-x})O_2$, and $Nb_{18}V_4O_{55}$	82.7	1/0.28/0.16	5.3% $Mo_1V_{0.45}O_x$ 10.7% $Nb_1V_{0.76}O_x$ 1.3% Σ

* Unreacted elements Mo, V, and Nb.

Table 2. Unit cell parameters of oxides with the rutile-type structure

Sample	Thermal treatment conditions		Unit cell parameters	
	T, °C	atmosphere	*a*, Å	*c*, Å
$V_{0.3}MoNb_{0.37}O_x$	550	He	4.788 ± 0.003	2.865 ± 0.003
$V_{0.3}MoNb_{0.37}O_x$	650	He	4.755 ± 0.005	2.874 ± 0.004
MoO_2 ICDD, PDF-2 [00-02-0422]	–	–	4.86	2.79
VO_2 ICDD, PDF-2 [00-44-0253]	–	–	4.554	2.855

Thermal treatment in air. Figure 1 shows the X-ray diffraction patterns of the sample of $V_{0.3}MoNb_{0.37}O_x$, which were measured in situ in the high-temperature chamber in air at 180–650°C (curves *2*–*8*).

The sample dried at 180°C was X-ray amorphous (Fig. 1, curve *2*). Only two broad and diffuse halos at the angles of 2θ ≈ 22° and 26°–27° were observed. Upon heating the sample to 300°C, an additional broad halo appeared at 2θ = 8° and the peaks at 22° and 26.5° became more intense (Fig. 1, curve *3*). Upon subsequent heating to 500°C, the maximum at 2θ = 22° became narrower and more intense; in this case, the line intensities at 2θ = 8° and 26.5° remained almost unchanged (Fig. 1, curves *4*, *5*). Upon heating to 550°C, reflections due to the Mo_5O_{14}-type structure appeared [ICDD, PDF-2, 00-012-0517, 00-031-1437, 00-027-1310], the theoretical X-ray diffraction pattern of which is shown in Fig. 1 (curve *1*), as calculated using the PCW program [32]. The unit cell parameters of this phase are a = 22.874 ± 0.002 Å and c = 4.015 ± 0.001 Å. As compared to the unit cell parameters of the Mo_5O_{14} oxide, a decrease in the parameter a and an increase in the parameter c were observed [29]. Analogous changes in the parameters occurred in the formation of Nb- or V-substituted molybdenum oxides with the Mo_5O_{14}-type structure [33, 34]. As the temperature was increased to 600 and 650°C, the lattice parameters of the ternary oxide phase remained unchanged.

At 650°C, an additional reflection appeared in the X-ray diffraction pattern at 2θ = 27.3° along with lines related to the Mo_5O_{14}-type structure and the intensity of the line at 2θ = 12.3° increased. This suggests the appearance of a MoO_3 oxide phase [ICDD, PDF-2, 00-

Table 3. Effect of thermal treatment conditions on the catalytic properties of $V_{0.3}Mo_1Nb_{0.27}O_x$ ($T_{reaction}$ = 400°C; the reaction mixture contained 5 vol % ethane, 6 vol % NH_3, 6 vol % O_2, and the balance N_2; the conversion of ethane was 10%)

Thermal treatment conditions		Phase composition	Selectivity, %		$w \times 10^9$ mol m^{-2} s^{-1}
T, °C	calcination atmosphere		$C_2H_4 + C_2H_3N$	CO_x	
400	Air	Unidimensionally ordered phase with d = 4.00 Å	98.0	2.0	11.6
500	Air	″	97.5	2.5	12.9
400	Reaction mixture	″	97.0	3.0	11.2
500	Reaction mixture	$(V_xMo_{1-x})O_2$ Unidimensionally ordered phase with d = 4.00 Å MoO_3 (traces)	80.1	19.9	4.3
500	Helium	$(V_xMo_{1-x})O_2$ Unidimensionally ordered phase with d = 4.00 Å	83.0	17.0	6.0

035-0609]. Because the differential dissolution data (Table 1) indicate that the composition and concentration of the ternary phase after thermal treatment at 650°C remained unchanged, as compared with the sample calcined in air at 550°C, we can conclude that the crystallization of impurity molybdenum oxides (less than 5% according to differential dissolution data) occurred at the specified temperatures. Table 1 compares the experimental X-ray diffraction data with chemical phase analysis data (differential dissolution data). It can be seen that, as the calcination temperature was increased from 300 to 550°C, the concentration of the ternary oxide phase increased. In this case, the composition of the oxide also changed: a decrease in the niobium content and an increase in the vanadium content were observed. This is consistent with previous data that the V–Mo–Nb oxide phase is formed based on a Nb–Mo compound [30]. As the temperature was increased from 550 to 650°C, the composition and concentration of this phase in the sample remained unchanged.

Transmission electron microscopy (TEM) data indicate that a unidimensionally ordered layered V–Mo–Nb compound was formed upon calcination at 400°C in air. Figure 2a shows a typical micrograph of a V–Mo–Nb–O particle. Micrometer-sized particles were composed of blocks of 5–10 nm in size, which have a layered structure with an interlayer spacing of ~400 Å. Individual blocks are disoriented and interlinked through interblock boundaries. Microdiffraction on these particles is characteristic of a unidimensionally ordered structure: the interplanar spacings d ~ 4.00 Å (001 reflection of the Mo_5O_{14}-type structure) and ~2.00 Å (002 reflection of the Mo_5O_{14}-type structure) and a diffuse halo at d = 3.47 Å, which was also observed in the X-ray diffraction pattern of the uncrystallized phase, were observed. According to microanalysis data, the composition of the V–Mo–Nb compound at various points of the particle varied over the range $V_{0.21–0.42}Mo_1Nb_{0.26–0.45}O_x$; however, on the average, it corresponded to the specified composition $V_{0.3}Mo_1Nb_{0.37}O_x$ and was in agreement with differential dissolution data (Table 1).

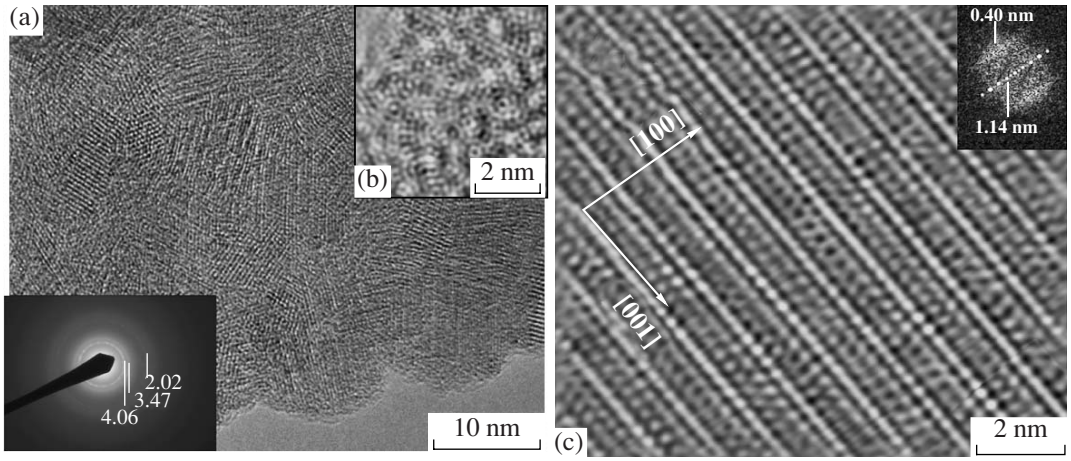

Fig. 2. Micrographs and electron diffraction patterns for the V–Mo–Nb–O compound calcined in air at (a, b) 400 and (c) 550°C.

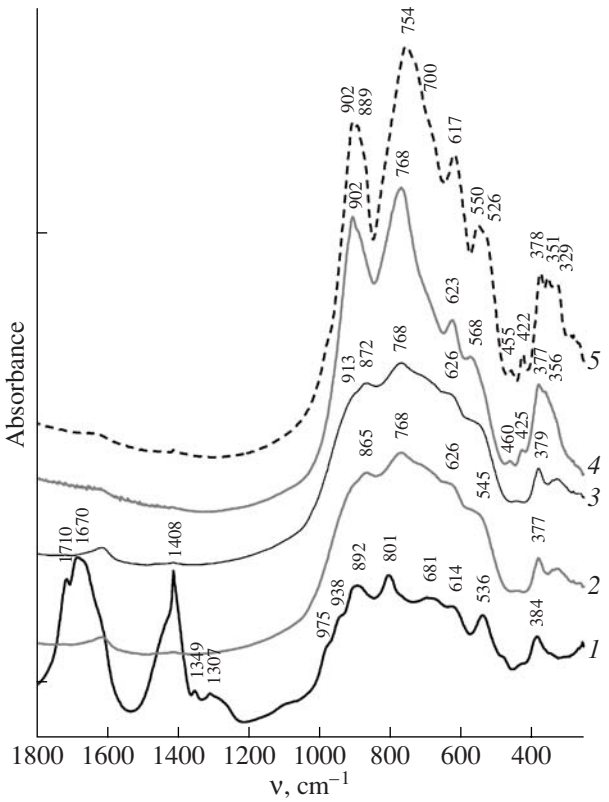

Fig. 3. IR spectra of $V_{0.3}Mo_1Nb_{0.27}O_x$ samples (*1*) dried at 180°C and calcined in a flow of air at (*2*) 300, (*3*) 400, or (*4*) 550°C and (*5*) the $(Mo_{0.6}Nb_{0.4})_5O_{14}$ sample (550°C).

A high-resolution micrograph exhibited approximately rounded clusters (Fig. 2b). Based on published data [35, 36], these clusters can be ascribed to Mo_5O_{14} structure fragments like stars that consists of a pentagonal bipyramid sharing edges with five octahedrons (see the structure of Mo_5O_{14} in Fig. 1). In an ideal structure, these elements joined at corners through individual octahedrons form a square in the *ab* plane. In the case of calcination in air at 400°C, stars were formed, but their ordering in the *ab* plane did not occur.

Figure 2c shows an electron micrograph of a crystalline particle of the sample calcined at $T = 550$°C with a tetragonal structure of the M_5O_{14} type (as demonstrated above by X-ray analysis). The crystal orientation relative to the beam is [010], as is proved by reflections in the Fourier diffraction pattern (Fig. 2c, inset) corresponding to a set of (100) planes with an interplanar spacing of ~11.4 Å (lattice parameter $a/2$ of M_5O_{14}) and (001) planes with an interplanar spacing of ~4 Å (lattice parameter c for M_5O_{14}). Arrows in the crystal structure image (Fig. 2c) indicate the directions of the *a* and *c* axes. According to EDAX data, the composition of the ternary compound was also nonuniform at 550°C: it varied in the range $V_{0.12–0.40}Mo_1Nb_{0.31–0.46}O_x$, although the average composition was $V_{0.3}Mo_1Nb_{0.37}O_x$.

Because the V–Mo–Nb oxide was amorphous or weakly crystallized up to a calcination temperature of 500°C, we studied $V_{0.3}Mo_1Nb_{0.37}O_x$ samples of calcined in air over the temperature range of 180–550°C using IR spectroscopy.

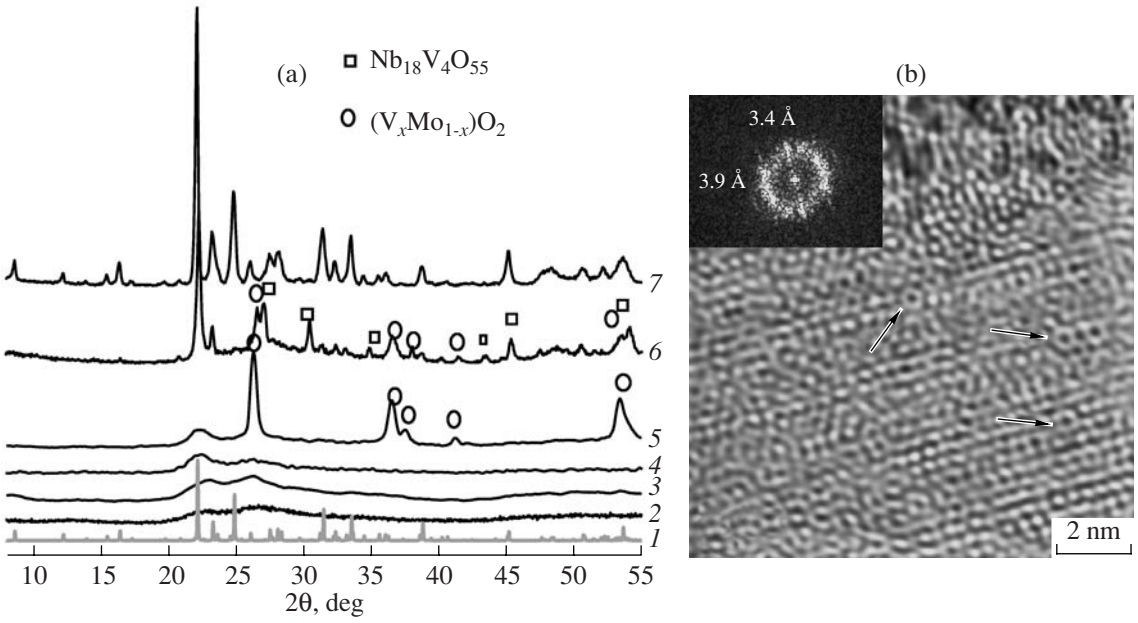

Fig. 4. (a) Diffraction patterns of $V_{0.3}Mo_1Nb_{0.37}O_x$ samples measured in a flow of helium depending on temperature: (*1*) theoretical X-ray diffraction pattern of Mo_5O_{14}, (*2*) 180°C, (*3*) 400°C, (*4*) 500°C, (*5*) 550°C, (*6*) 650°C, and (*7*) 550°C in air after calcination in helium at 550°C: (O) phase with the rutile structure; (□) $Nb_{18}V_4O_{55}$; diffraction lines due to a Mo_5O_{14}-type phase are unmarked. (b) Micrograph of a $V_{0.18}Mo_1Nb_{0.38}O_x$ particle ($T = 650$°C).

The IR spectrum of the sample dried at 180°C (Fig. 3, curve *1*) exhibited intense absorption bands at 1700–1600 cm^{-1}, which correspond to the ν(C=O) of the oxalate ion and the δ(OH) of water, an absorption band at 1408 cm^{-1} due to ammonium ion vibrations [37], and absorption bands characteristic of the stretching and deformation vibrations of M–O bonds (at 975, 938, 892, 801, 681, 614, 538, and 384 nm) [37]. Bondareva et al. [30] found that, in $V_{0.3}MoNb_{0.27}O_x$, niobium oxalate was hydrolyzed to form a hydrated niobium oxide under catalyst preparation conditions; the formation of vanadium and molybdenum oxalates was detected using NMR spectroscopy. Based on an analogy of the IR spectra, we assumed that the formation of the V–Mo–Nb oxide with the formula $V_{0.3}MoNb_{0.37}O_x$ occurred analogously to that considered previously [30] and suggested the presence of undecomposed mixed polymetallic ammonium salts and vanadium and molybdenum oxalates at $T = 180$°C [30].

An increase in the calcination temperature to 300°C resulted in the decomposition of precursor salts: absorption bands characteristic of the oxalate ion and NH_4^+ disappeared from the IR spectra. In this case, the spectrum in the region of M–O vibrations changed (Fig. 3, curve *2*), and three broad peaks appeared in the X-ray diffraction pattern at the angles 2θ = 8°, 22°, and 26.5°. An increase in the calcination temperature to 400°C was accompanied by an insignificant shift of the IR absorption bands (Fig. 3, curve *3*). In this case, two halos at 2θ = 22° and 27° became more clearly pronounced in the X-ray diffraction pattern. The IR spectrum of the sample calcined at 550°C (Fig. 3, curve *4*) exhibited shifts, a narrowing, and an increase in the intensities of absorption bands in the region of M–O vibrations. Taking into account the fact that, according to X-ray diffraction data, only the Mo_5O_{14}-type structure is formed at the specified temperature in air, the bands at 902, 768, 623, 568, 460, 425, 377, and 329 cm^{-1} can be ascribed to the V–Mo–Nb compound with this structure. For comparison, Fig. 3 (curve *5*) shows the spectrum of the Mo–Nb oxide $(Mo_{0.6}Nb_{0.4})_5O_{14}$, which is analogous to the spectrum of a V–Mo–Nb compound. The observed band shift in the spectrum of a single-phase V–Mo–Nb sample with respect to lines in the spectrum of the Nb–Mo compound can be interpreted as the result of vanadium insertion into the Nb–Mo oxide structure, on the basis of which a ternary oxide phase is formed [30]. Note that, in general, the shape of the spectra of the sample calcined in the temperature range of 300–550°C remained unchanged. Broad low-intensity absorption bands observed in the spectra at temperatures lower than 500°C can be due to amorphous and disordered V–Mo–Nb oxide phases formed.

Thermal treatment in a mixture of He + 0.3% O_2. In the course of thermal treatment in a mixture of He + 0.3% O_2, the formation of the model sample $V_{0.3}MoNb_{0.37}O_x$ occurred via the same steps as in the thermal treatment in air (see Fig. 1). At 550°C, a Mo_5O_{14}-type structure was formed, whereas lines due to the MoO_3 oxide and trace amounts of $Nb_{18}V_4O_{55}$ [ICDD, PDF-2, 00-046-0087] appeared on heating to 650°C. The appearance of the above phases was due to the crystallization of Mo, V, and Nb impurity compounds, the amount of which was no higher than 5% according to differential dissolution data (Table 1).

Thermal treatment in helium. Figure 4a shows the X-ray diffraction patterns of a dried sample measured in a flow of helium in the high-temperature X-ray chamber at 180, 400, 500, and 550°C (curves *2–5*) and a sample calcined in the reactor (ex situ) in helium at 650°C (curve *6*).

Upon heating to 400°C, as well as upon calcination in air, three broad halos at 2θ = 8°, 22°, and 26° were observed (Fig. 4a, curve *3*). At 500°C, the intensity of the line at 2θ = 22° increased and this line narrowed with the retention of two halos at 2θ = 8· and 26° (Fig. 4a, curve *4*). An increase in the temperature to 550°C resulted in the appearance of additional reflections at 2θ = 26.30°, 36.80°, 37.50°, 41.35°, and 53.40°, which belong to a rutile-type structure [ICDD, PDF-2, 00-002-0422, 00-044-0253] (Fig. 4a, curve *5*). As the temperature was increased to 650°C, in addition to these lines, reflections also appeared at 2θ = 20.8°, 27.0°, 30.5°, 33.0°, and 34.9°, which can be attributed to the compound $Nb_{18}V_4O_{55}$. The observed deviations of calculated unit cell parameters for the last phase (a = 7.99 Å, b = 16.81 Å, and c = 17.15 Å) may be due to stoichiometry changes, as additionally supported by differential dissolution data (Table 1).

Unlike calcination in air at 550°C, the crystallization of the V–Mo–Nb phase did not occur in helium at this temperature, although the amount of the $Mo_1V_{0.20}Nb_{0.41}$ phase was 84% according to differential dissolution data (Table 1). The high niobium content of the ternary oxide phase was due to the formation of a V–Mo phase with the rutile structure and, consequently, molybdenum and vanadium deficiency in the V–Mo–Nb oxide. A Nb–V oxide was formed at 650°C; in this case, the amount of niobium as a ternary oxide constituent decreased, as compared with the sample calcined at 550°C (see Table 1). Note that even at 650°C the ternary oxide exhibited a unidimensionally ordered structure (see Fig. 4), which is characterized by interplanar spacings of d = 4.00 and 2.00 Å. As the temperature was increased from 400 to 650°C, the halfwidths of 00l reflections (d = 4.00 and 2.02 Å) in the diffraction patterns changed; that is, the block sizes in the [001] direction changed from 7 nm at 400°C to 60 nm at 650°C. This corresponds to an increase in the number of layers in the block from ~20 to ~150. However, the layers remained disordered, as evidenced by the absence of the complete set of lines corresponding to the Mo_5O_{14}-type structure from the diffraction pattern.

Transmission electron microscopic data suggest that a unidimensionally ordered layered V–Mo–Nb compound was formed at 400–550°C in helium. Typical micrographs of particles are similar to the micrographs of the unidimensionally ordered layered V–Mo–Nb compound prepared by calcination in air at 400°C (see Fig. 2a).

As in the thermal treatment in air at 400°C, rounded metal–oxygen clusters can be seen in the micrographs of a sample calcined in helium at 650°C. These clusters did not form an ideal structure, and they were unoriented with respect to one another. Microdiffraction exhibited interplanar distances of 4.00 and 2.00 Å and a diffuse peak at $d \sim 3.4$ Å. Thus, in the (001) plane, the structure remained disordered up to 650°C. In this case, in the perpendicular (010) plane, the number of layers in blocks increased, and this increase manifested itself in an increase in the intensity and a narrowing of the (001) and (002) lines in the X-ray diffraction pattern of the sample calcined at 650°C.

Table 2 summarizes the unit cell parameters of the oxide with the rutile-type structure in samples calcined in helium at $T = 550$ and 650°C and lattice parameters for MoO_2 and VO_2 oxides [ICDD, PDF-2, 00-002-0422, 00-044-0253]. A comparison between experimental and published data showed a decrease in the unit cell parameter a and an increase in the parameter c for the phase with the rutile-type structure in the calcined samples. It is believed that structural distortions were due to the insertion of vanadium into the MoO_2 oxide structure because it is well known that V^{4+} and Mo^{4+} oxides can form solid solutions with mutual solubility [38, 39]. A transmission microscopic study demonstrated the occurrence of particles of the V–Mo phase with a nonuniform distribution of V in their bulk. According to EDAX analysis, the composition of the V–Mo compound varied over a wide range: $V_{0.11–0.7}Mo_1O_x$.

Note that, if a flow of helium was replaced by air at $T = 550$°C, only a V–Nb–Mo oxide with the Mo_5O_{14}-type structure was formed with the average chemical formula $V_{0.3}MoNb_{0.37}O_x$ (Fig. 4a, curve *7*), which was characterized by a full set of diffraction lines for this phase.

DISCUSSION

Based on the above data, we can conclude that the formation of a ternary V–Mo–Nb oxide, where the ratio $M^{5+}/Mo^{6+} = 2/3$ corresponds to the ratio between pentavalent and hexavalent cations in the Mo_5O_{14} structure, began even at 300°C. The decomposition of starting salts and the formation of an amorphous oxide phase occurred. In this case, the V–Mo–Nb–O structure was formed on the basis of the $Nb_2Mo_3O_{14}$ matrix; the absorption bands of this matrix could be detected in the IR spectra (Fig. 3) immediately after the decomposition of salt species and up to $T = 650$°C. At temperatures lower than 550°C, this phase was disordered; it was characterized by a maximum at $2\theta = 22°$ ($d = 4.00$ Å) and two halos at $2\theta = 8°$ and 26° in the X-ray diffraction patterns (Fig. 1). Particle aggregates of unidimensionally ordered disoriented blocks with an interplanar spacing of ~4.00 Å and a block size of <10 nm can be seen in the micrograph (Fig. 2a). For Mo-containing structures, an interplanar spacing of 4.00 Å is characteristic of the M–M or O–O distance in corner-sharing octahedra [39]. Thus, we assume that oxygen polyhedra from different layers are joined corner to corner. In the layer plane, the arrangement of polyhedra is disordered; therefore, lines with the indices (*hkl*) and (*hk*0) were absent from the diffraction pattern, although clusters of the elements of the future M_5O_{14} structure as individual stars, which consisted of pentagonal bipyramids sharing edges with five octahedra, were formed (see Fig. 2b). Because of the unformed structure, the chemical composition of individual V–Mo–Nb oxide particles varied over the range of $V_{0.21–0.42}Mo_1Nb_{0.26–0.45}O_x$ (EDAX analysis data) but, on average, corresponded to the specified chemical formula $V_{0.3}Mo_1Nb_{0.37}O_x$. Nanocrystal structures of this kind were also observed in V–Mo–W catalysts for acrolein oxidation to acrylic acid; a $(Mo,V,W)_5O_{14}$ mixed oxide was formed upon the calcination of these catalysts in air [18, 19].

At 550°C, the crystallization of a V–Mo–Nb ternary oxide occurred in air. In this case, the X-ray diffraction pattern exhibited the entire set of diffraction peaks corresponding to a structure like M_5O_{14}, where M = Mo, V, or Nb, which is shown in Fig. 1. According to differential dissolution, X-ray diffraction, and transmission electron microscopic data, the structure was retained without degradation upon thermal treatment in air up to 650°C.

As distinct from calcination in air, the crystallization of a ternary oxide with the M_5O_{14} structure did not occur in a flow of helium, whereas a three-component compound with a unidimensionally ordered structure composed of disoriented blocks characterized by the interplanar spacing $d = 4.00$ Å (see Fig. 4) was formed up to 650°C. In this case, as the temperature was increased, the diffraction patterns exhibited a change in the halfwidth of the 00*l* reflections ($d = 4.00$ Å), which corresponded to a change in block sizes in the [001] direction from 7 nm at 400°C to 60 nm at 650°C. However, the layers remained disordered. Moreover, upon calcination in a flow of helium, a large amount of reduced V^{4+} and Mo^{4+} cations was formed; these cations formed an individual phase of $(V_xMo_{1-x})O_2$, which was observed using both diffraction techniques and differential dissolution or electron microscopy (see Table 1). Consequently, the composition of the ternary compound was deficient in molybdenum and vanadium, as was found using differential dissolution (Table 1). It is likely that, in a flow of helium, the molybdenum and vanadium ions were reduced by ammonium and oxalate ions released upon the decomposition of the starting salts (ammonium paramolybdate, ammonium metavanadate, and niobium oxalate). The reduction of vanadium and molybdenum ions due

to the decomposition of ammonium salts was also observed in the formation of vanadium–molybdenum catalysts [40, 41].

The experiments performed in He + 0.3%O_2 demonstrated that even a relatively low oxygen concentration in the thermal treatment atmosphere facilitated the reoxidation of molybdenum(IV) and vanadium(IV), which were formed upon calcination in pure helium, to cause the formation of compounds analogous to the compounds prepared by sample calcination in air. It is likely that, in previous studies [8, 10], inadequate control of the oxygen content of the inert gas resulted in dramatically different data on the activity of chemically similar samples calcined in an inert atmosphere.

The change in the phase composition under varied thermal treatment conditions was accompanied by changes in catalytic properties. A comparison between kinetic characteristics and phase compositions (see Table 3) suggested that samples prepared by calcination at T = 400–450°C in both oxidizing and inert atmospheres or in a reaction mixture exhibited the best catalytic properties. The active component was a unidimensionally ordered layered structure with Mo_5O_{14}-type structure elements. An increase in the temperature in the inert atmosphere or the reaction mixture facilitated the reduction of a portion of molybdenum and vanadium ions to V^{4+} and Mo^{4+} states and the formation of the $(V_xMo_{1-x})O_2$ solid solution. This resulted in a decrease in the activity of samples and in selectivity for partial oxidation products; this is consistent with published data on the destructive oxidation of alkanes by MoO_2 [15].

Thus, we found that the formation of active V–Mo–Nb–O catalysts upon thermal treatment up to 500°C proceeds via the same irreversible steps regardless of the atmosphere, whereas the atmosphere of thermal treatment at ≥500°C has an effect on the phase composition of the catalyst and its catalytic properties.

ACKNOWLEDGMENTS

This work was supported by the Russian Foundation for Basic Research (project nos. 07-03-00203 and 05-03-32236).

REFERENCES

1. Smejkal, Q., Linke, D., and Baerns, M., *Chem. Eng. Proc.*, 2005, vol. 44, p. 421.
2. Brazdil, J.F., *Top. Catal.*, 2006, vol. 38, no. 4, p. 421.
3. Grassilli, R.K., *Catal. Today*, 1999, vol. 49, p. 141.
4. Labinger, J.A., *J. Mol. Catal. A: Chem.*, 2004, vol. 220, p. 27.
5. Thorsteinson, E.M., Wilson, T.P., Young, F.G., and Kasai, P.H., *J. Catal.*, 1978, vol. 52, no. 5, p. 116.
6. Burch, R. and Swarnakar, R., *Appl. Catal.*, 1991, vol. 70, p. 129.
7. Desponds, O., Keiski, R.L., and Somorjai, G.A., *Catal. Lett.*, 1993, vol. 19, p. 17.
8. Botella, P., Lopez Nieto, J.M., Dejoz, A., Vazquez, M.I., and Martinez-Arias, A., *Catal. Today*, 2003, vol. 78, p. 507.
9. Bondareva, V.M., Andrushkevich, T.V., Aleshina, G.I., Plyasova, L.M., Dovlitova, L.S., Lapina, O.B., Khabibulin, D.F., and Vlasov, A.A., *React. Kinet. Catal. Lett.*, 2006, vol. 87, no. 2, p. 377.
10. Merzuoki, M., Taouk, B., Monceaux, L., Bordes, E., and Courtine, P., *Stud. Surf. Sci. Catal.*, 1992, vol. 72, p. 165.
11. Roussel, M., Bouchard, M., Bordes-Richard, E., Karim, K., and Al-Sayari, S., *Catal. Today*, 2005, vol. 99, p. 77.
12. Roussel, M., Bouchard, M., Karim, K., Al-Sayari, S., and Bordes-Richard, E., *Appl. Catal., A*, 2006, vol. 308, p. 62.
13. Ruth, K.K.R. and Burch, R., *J. Catal.*, 1998, vol. 175, p. 16.
14. Al-Saeedi, J.N., Vasudaen, V.K., and Guliants, V.V., *Catal. Commun.*, 2003, vol. 4, p. 537.
15. Botella, P., Lopez, NietoJ.M., Concepcion, P., and Vazquez, M.I., *Appl. Catal., A*, 2006, vol. 298, p. 16.
16. Ueda, W., Chen, N.F., and Oshihara, K., *Chem. Commun.*, 1999, vol. P, p. 517.
17. Ueda, W. and Oshihara, K., *Appl. Catal., A*, 2000, vol. 200, nos. 1-2, p. 135.
18. Knobl, S., Zenkovets, G.A., Kryukova, G.N., Ovsitser, O., Niemeyer, D., Schlogl, R., and Mestl, G., *J. Catal.*, 2003, vol. 215, p. 177.
19. Zenkovets, G.A., *Doctoral (Chem.) Dissertation*, Novosibirsk: Inst. of Catalysis, 2004.
20. Al-Saeedi, J.N., Guliants, V.V., Guerrero-Perez, O., and Banares, M.A., *J. Catal.*, 2003, vol. 215, p. 108.
21. Asakura, K.N.K., Kubota, T., and Iwasawa, Y., *J. Catal.*, 2000, vol. 194, p. 309.
22. Holmes, S.A., Al-Saeedei, J., Gulians, V.X., Boolchand, P., Geodiev, D., and Hackler, U., *Catal. Today*, 2001, vol. 67, no. 4, p. 403.
23. Lopez Nieto, J.M., Botella, P., Concepcion, P., Dejoz, A., and Vazquez, M.I., *Catal. Today*, 2004, vols. 91–92, p. 241.
24. US Patent 5 472 925, 1995.
25. Grasselli, R.K., Buttrey, D.J., DeSanto, P.J., Burrington, J.D., Lugmair, C.G., Volpe, A.F., and Weingand, T.S., *Catal. Today*, 2004, vols. 91–92, p. 251.
26. US Patent 6350716, 2002.
27. US Patent 6399816, 2002.
28. US Patent 6383977, 2002.
29. Kihlborg, L., *Ark. Kemi*, 1963, vol. 21, p. 427.
30. Bondareva, V.M., Andrushkevich, T.V., Aleshina, G.I., Maksimovskaya, R.I., Plyasova, L.M., Dovlitova, L.S., and Burgina, E.B., *React. Kinet. Catal. Lett.*, 2006, vol. 88, no. 1, p. 183.
31. Malakhov, V.V. and Vlasov, A.A., *Kinet. Catal.*, 1995, vol. 36, p. 503.

32. Klaus, W. and Nolze, G., *J. Appl. Crystallogr.*, 1996, vol. 29, p. 301.

33. Ekstrom, T. and Nygen, M., *Acta Chem. Scand.*, 1972, vol. 26, p. 1827.

34. Ekstrom, T. and Nygen, M., *Acta Chem. Scand.*, 1972, vol. 26, p. 1836.

35. Werner, H., Timpe, O., Herein, D., Uchida, Y., Pfander, N., Wild, U., and Shlogl, R., *Catal. Lett.*, 1997, vol. 44, p. 153.

36. Botella, P., Garcia-Gonzalez, E., Lopez Nieto, J.M., and Gonzalez-Calbet, J.M., *Solid State Sci.*, 2005, vol. 7, p. 507.

37. Nakomoto, K., *Infrared Spectra of Inorganic and Coordination Compounds*, London: Wiley, 1963.

38. Londo, J.M. and Kierkegaard, P.A., *Acta Chem. Scand.*, 1970, vol. 24, p. 420.

39. Porai-Koshits, M.A. and Atovmyan, L.O., *Kristallokhimiya i stereokhimiya koordinatsionnykh soedinenii molibdena* (Crystal Chemistry and Stereochemistry of Coordination Compounds of Molybdenum), Moscow: Nauka, 1974.

40. Olen'kova, I.P., *Cand. Sci. (Chem.) Dissertation*, Novosibirsk: Inst. of Catalysis, 1982.

41. Plyasova, L.M., *Doctoral (Chem.) Dissertation*, Novosibirsk: Inst. of Catalysis, 1993.